FAST SPATIALLY VARIANT DECONVOLUTION FOR OPTICAL MICROSCOPY VIA ITERATIVE SHRINKAGE THRESHOLDING

Nikhil Chacko, Michael Liebling

Department of Electrical and Computer Engineering
University of California, Santa Barbara, CA 93106, U.S.A.

ABSTRACT

Deconvolution offers an effective way to improve the resolution of optical microscopy data. While fast algorithms are available when the point spread function (PSF) is shift-invariant (SI), they are not directly applicable in thick samples, where the problem is shift-variant (SV). Here, we propose a fast iterative shrinkage/thresholding 3D deconvolution method that uses different PSFs at every depth. This is realized by modeling the imaging system as a multi-rate filter-bank, with each channel corresponding to a distinct 3D PSF dependent on the position along the optical axis. The complexity associated with the thresholded Landweber update in each iteration of our SV algorithm is equivalent to that of an iteration in an SI algorithm, multiplied by the number of channels in the filter-bank. We simulated images of a set of beads embedded in an aqueous gel, using varying PSFs along the optical axis, to illustrate the effectiveness of our algorithm.

***Index Terms*—** Optical microscopy, spatially-variant deconvolution, wavelets, sparsity, fast iterative shrinkage/thresholding algorithms (FISTA).

1. INTRODUCTION

Optical microscopy is an important tool for imaging live samples. Volumetric, three-dimensional (3D) imaging is possible in weakly-scattering objects by collecting a stack of images while focusing the microscope objective at different depths in the sample. In wide-field microscopy, images are contaminated by out-of-focus light from planes above and below the examined plane. This results in a spatial blur, particularly in the axial direction. The image formation process is usually modeled as a linear space-invariant (SI) operation, where the 3D object is magnified and convolved with the response of an impulse, the point spread function (PSF). The 3D object can be restored via multiple algorithms [1], including the classic Landweber deconvolution method [2]. While the space-invariance assumption is reasonable for relatively thin samples, when imaging thicker samples, the shape of the PSF varies with depth, particularly when there is a mismatch between the refractive indices of the immersion medium (n_i), any cover-slip (n_g) and sample (n_s) (Fig. 1).

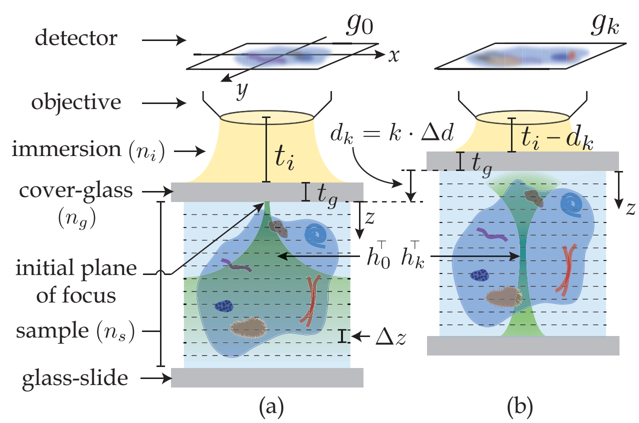

Fig. 1. Each 2D plane imaged during optical sectioning, g_k, can be modeled as an inner-product (along z) between the original 3D data stack f_{orig} and the depth-varying PSF $h_k^\top$.

To restore images obtained with depth-dependent PSFs, several algorithms have been proposed that involve breaking the dataset into smaller blocks on which efficient SI deconvolution algorithms can be applied [4, 5]. The quality of such approaches depends on the size of the blocks and the careful design of transition masks to merge them once deconvolved. Other approaches approximate the depth-varying blur as a spatially weighted combination of SI convolutions [3, 6]. In this paper, we present an approach that directly considers a depth-variant PSF deconvolution problem, yet preserves the form of a highly efficient SI deconvolution method. Specifically, we model the imaging system as a multi-rate filter bank, where each plane along the optical axis is assigned to a channel with a different PSF; the filter bank structure leads to a Landweber deconvolution that uses an *iterative-shrinkage/thresholding* algorithm (ISTA).

This paper is organized as follows. In Section 2, we introduce the image formation model and the inverse problem. In Section 3, we describe the proposed method. In Section 4, we characterize the algorithm on simulated images. Finally, we discuss the algorithm and conclude in Section 5.

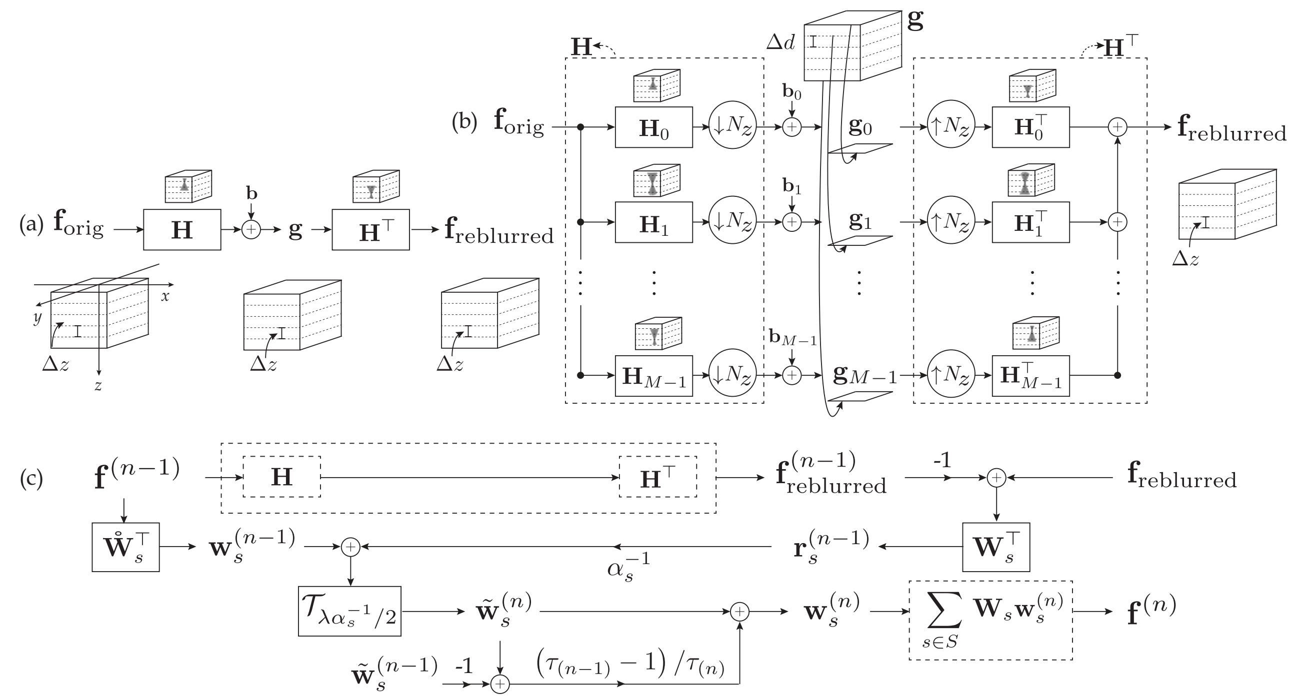

Fig. 2. Block diagram of shift-invariant FISTA deconvolution (SI-FISTA, (a)+(c)) and proposed shift-variant FISTA deconvolution (SV-FISTA = (b) + (c)). Both algorithms are based on a *reblurring* operation and Landweber iterations: (a) reblurring in SI-FISTA [7, 8]; (b) reblurring in proposed SV-FISTA; (c) thresholded Landweber deconvolution: the structure and complexity of the thresholding stage remains the same for SI-FISTA and SV-FISTA. (See text for descriptions of variables and symbols.)

2. PROBLEM STATEMENT

We consider a 3D object with local intensity $f_{\text{orig}}(\mathbf{x}, z)$, $\mathbf{x} = (x, y) \in \mathbb{R}^2, z \in \mathbb{R}$, imaged with a system characterized by 3D PSFs $h_k(\mathbf{x}, z)$ that are dependent on the axial position (depth) of the microscope stage $d_k = k\Delta d$, where Δd is the step by which the stage is moved between the acquisition of each slice. The 2D blurred image on the camera for stage position $d = d_k$ can then be modeled as:

$$g_k(\mathbf{x}) = \iiint f_{\text{orig}}(\boldsymbol{\xi}, \eta) h_k^\top(\boldsymbol{\xi} - \mathbf{x}, \eta) \mathrm{d}\boldsymbol{\xi} \mathrm{d}\eta + b_k(\mathbf{x}), \quad (1)$$

for $k = 0, \dots, M-1$ measured slices, where $h_k^\top(\mathbf{x}, z) \triangleq h_k(-\mathbf{x}, -z)$ and b_k denotes additive measurement noise. Note that this model is laterally- but not axially-shift-invariant since we do not require $h_k(\mathbf{x}, z) = h_0(\mathbf{x}, d_k + z)$.

We sample f_{orig} and h_k on a discrete 3D grid with $N_x \times N_y \times N_z$ voxels, with lateral and axial sampling steps $\Delta\mathbf{x}$ and Δz, respectively. Similarly, we sample g_k to form an $N_x \times N_y$ image, with lateral sampling step $\Delta\mathbf{x}$. Note that the stage position $k\Delta d$ (associated to image g_k) can be different from $k\Delta z$ (the position of the kth slice in f_{orig}) [9]. This mismatch is captured by the space variant PSF model, which we assume is known a priori. After discretization, Eq. (1) becomes:

$$\mathbf{g} = \mathbf{H}\mathbf{f}_{\text{orig}} + \mathbf{b}, \quad (2)$$

or, further expanded to reveal the matrices for each slice:

$$\begin{bmatrix} \mathbf{g}_0 \\ \vdots \\ \mathbf{g}_{M-1} \end{bmatrix} = \begin{bmatrix} \mathbf{D}\mathbf{H}_0 \\ \vdots \\ \mathbf{D}\mathbf{H}_{M-1} \end{bmatrix} \mathbf{f}_{\text{orig}} + \begin{bmatrix} \mathbf{b}_0 \\ \vdots \\ \mathbf{b}_{M-1} \end{bmatrix}, \quad (3)$$

where $\mathbf{H}_k$ are $(N_x \cdot N_y \cdot N_z) \times (N_x \cdot N_y \cdot N_z)$-sized block-circulant matrices (for 3D circular convolution with h_k), $\mathbf{D}$ is the $(N_x \cdot N_y) \times (N_x \cdot N_y \cdot N_z)$-sized down-sampling matrix that selects only the first z-plane of $\mathbf{H}_k\mathbf{f}_{\text{orig}}$, and where $\mathbf{g}_k, \mathbf{f}_{\text{orig}}$ and $\mathbf{b}_k$ are vectors containing lexicographically arranged samples of g_k, f_{orig} and b_k, respectively.

The inverse problem is to find an estimate $\bar{\mathbf{f}}$ of $\mathbf{f}_{\text{orig}}$, given $\mathbf{g}$ and $\mathbf{H}$. We follow a transform-domain sparsity-based reconstruction approach [10, 7, 8] that assumes $\mathbf{f}_{\text{orig}}$ has a sparse wavelet representation $\mathbf{f}_{\text{orig}} = \mathbf{W}\mathbf{w}_{\text{orig}}$, where $\mathbf{W}$ is the synthesis matrix whose columns are the elements of the wavelet basis and $\mathbf{w}_{\text{orig}}$ is a set of (sparse) wavelet coefficients. The estimate $\bar{\mathbf{f}} = \mathbf{W}\bar{\mathbf{w}}$ is found through minimization of the cost function:

$$\mathcal{C}(\mathbf{w}) \triangleq \|\mathbf{g} - \mathbf{H}\mathbf{W}\mathbf{w}\|_2^2 + \lambda\|\mathbf{w}\|_1, \quad (4)$$

$$= \sum_{k=0}^{M-1} \|\mathbf{g}_k - \mathbf{D}\mathbf{H}_k\mathbf{W}\mathbf{w}\|_2^2 + \lambda\|\mathbf{w}\|_1, \quad (5)$$

where $\|\bullet\|_p$ is the ℓ_p-norm operator and λ is a non-negative scalar quantity controlling wavelet regularization. Efficient solutions to problem (5) have been proposed when $\mathbf{H}$ is block circulant using Shannon [7] and generic wavelet bases [8] with the sub-band dependent ISTA (Fig. 2 (a) and (c)). We previously showed that this method remained applicable (with minimal computational overhead) in the context of multi-view microscopy [11]. Although our axially SV deconvolution problem has the form of a multi-channel filter bank, the down- and up-sampling operations (Fig. 2 (b)) require additional adjustments for the implementation to be efficient, as detailed in the section below.

3. METHOD

Vonesch and Unser [7, 8] have introduced an efficient multi-level sub-band dependent ISTA solution to the minimization problem (5) by considering the wavelet decomposition $\mathbf{f} = \mathbf{W}\mathbf{w} = \sum_{s\in\mathcal{S}} \mathbf{W}_s\mathbf{w}_s$, where $\mathbf{w}_s = \mathring{\mathbf{W}}_s^\top\mathbf{f}$ denotes the wavelet coefficients in the sub-band $s \in S$ (set of all sub-bands) that is characterized by its analysis and synthesis matrices $\mathring{\mathbf{W}}_s$ and $\mathbf{W}_s$, respectively. The ISTA solution involves alternating between two steps: (i) a Landweber update of the wavelet coefficients from the previous iteration, and (ii) wavelet sub-band weighted soft-thresholding of the coefficients computed in (i). The performance of ISTA can be further sped up by computing the next iterate based not only on the previous one, but also on two or more previously computed iterates (fast ISTA, (FISTA) [12]). Specifically, the steps of the minimization are:

$$\mathbf{w}_s^{(n)} = \tilde{\mathbf{w}}_s^{(n)} + \left(\frac{\tau_{(n-1)} - 1}{\tau_{(n)}}\right)\left(\tilde{\mathbf{w}}_s^{(n)} - \tilde{\mathbf{w}}_s^{(n-1)}\right), \quad (6)$$

where $\mathbf{w}_s^{(n)}$ are the wavelet coefficients in the sub-band s during the n-th iteration, and the temporary coefficients:

$$\tilde{\mathbf{w}}_s^{(n)} = \mathcal{T}_{\lambda\alpha_s^{-1}/2}\left\{\mathbf{w}_s^{(n-1)} + \alpha_s^{-1}\mathbf{r}_s^{(n-1)}\right\}, \quad (7)$$

are obtained via the soft-thresholding operation:

$$\mathcal{T}_\theta(w) \triangleq \operatorname{sgn}(w)\max\left(|w| - \theta, 0\right), \quad (8)$$

(with sgn denoting the signum function) after subtracting the residuals:

$$\mathbf{r}_s^{(n-1)} \triangleq \mathbf{W}_s^\top\mathbf{H}^\top\left(\mathbf{g} - \mathbf{H}\sum_{s'\in S}\mathbf{W}_{s'}\mathbf{w}_{s'}^{(n-1)}\right), \quad (9)$$

with weighing factors:

$$\tau_{(n)} = \frac{1 + \sqrt{1 + 4\tau_{(n-1)}^2}}{2}, \quad (10)$$

$$\alpha_s \geq \sum_{s'\in S_j}\rho\left(\mathbf{W}_{s'}^\top\mathbf{H}^\top\mathbf{H}\mathbf{W}_s\right), \quad s \in S_j. \quad (11)$$

The latter weights for sub-bands $s \in S_j$ (set of all sub-bands in scale j) are obtained from the spectral radius operator $\rho(\mathbf{A})$[13] (with $\mathbf{A}^\top$ denoting the complex-conjugate transpose of $\mathbf{A}$). These weights greatly accelerate convergence [8]. Commonly used initial conditions include $\tau_{(0)} = 1$ and $\tilde{\mathbf{w}}_s^{(0)} = \mathbf{w}_s^{(0)} = \mathring{\mathbf{W}}_s^\top\mathbf{g}$. The block diagram of this minimization approach is summarized in Fig. 2.

The matrix formulation is only formal as the matrices' large sizes are computationally prohibitive in practice. Nevertheless, efficient implementations of this algorithm have been derived when $\mathbf{H}^\top\mathbf{H}$ is block circulant [7, 8, 11], which, however, is not the case for the SV problem at hand (due to the axial downsampling-upsampling operations). We therefore derived efficient ways to compute (a) $\mathbf{H}^\top\mathbf{H}$, and (b) the sub-band dependent weighting constants α_s. Although $\mathbf{H}^\top\mathbf{H}$ is not block-circulant, each $\mathbf{H}_k$ is block-circulant and all operations executed in the analysis and synthesis side of the filter-bank can still be computed using only point-wise multiplications and additions using 3D discrete Fourier transforms (DFT). Specifically, the equivalent implementation of $\mathbf{f}_{\text{reblurred}} = \mathbf{H}^\top\mathbf{g}$ and $\mathbf{f}_{\text{reblurred}}^{(n)} = \mathbf{H}^\top\mathbf{H}\mathbf{f}^{(n)}$ using 2D/3D DFTs is given by:

$$\hat{f}_{\text{reblurred}}[\mathbf{u}, w] = \sum_{k=0}^{M-1}\hat{g}_k[\mathbf{u}]\cdot\hat{h}_k^*[\mathbf{u}, w], \quad (12)$$

$$\hat{f}_{\text{reblurred}}^{(n)}[\mathbf{u}, w] = \sum_{k=0}^{M-1}\left(\sum_{\ell=0}^{N_z-1}\frac{\hat{h}_k[\mathbf{u},\ell]\cdot\hat{f}^{(n)}[\mathbf{u},\ell]}{N_z}\right)\hat{h}_k^*[\mathbf{u}, w], \quad (13)$$

where $\hat{a}$ (and $\hat{a}^*$) denotes the 2D/3D DFT (and its complex-conjugate) of discrete image/volume a, $\mathbf{u} = [u, v]$, for $0 \leq u < N_x$, $0 \leq v < N_y$, and $0 \leq w < N_z$. Using similar expressions, we determine the sub-band dependent weights α_s in (11) using the power method [13] for an undecimated wavelet decomposition as:

$$\alpha_s = \lim_{m\to\infty}\sum_{s'\in S_j}\frac{\sum_{\mathbf{u},w}\left(\hat{b}\cdot\hat{a}_{s',s}^{(m)}\right)[\mathbf{u}, w]}{\sum_{\mathbf{u}',w'}\left(\hat{b}\cdot\hat{a}_{s',s}^{(m-1)}\right)[\mathbf{u}', w']}, \quad (14)$$

$$\hat{a}_{s',s}^{(m)}[\mathbf{u}, w] \triangleq \sum_{k=0}^{M-1}\left(\sum_{\ell=0}^{N_z-1}\frac{\left(\hat{h}_k\cdot\hat{\psi}_s\cdot\hat{a}_{s',s}^{(m-1)}\right)[\mathbf{u},\ell]}{N_z}\right) \cdot\left(\hat{\psi}_{s'}^*\cdot\hat{h}_k^*\right)[\mathbf{u}, w], \quad (15)$$

where $\hat{\psi}_s$ denotes the DFT of the wavelet or scaling function that spans the subspace associated with sub-band s, while $\hat{b}$ and $\hat{a}_{s',s}^{(0)}$ are random (nonzero) signals. This can be readily extended for a wavelet decomposition scheme with dyadic subsampling by aliasing the frequency components of $\hat{a}_{s',s}^{(m)}$ ($s', s \in S_j$) in (15) to be periodic by $N_x/2^j, N_y/2^j$ and $N_z/2^j$, along x, y and z, respectively. Good estimates of α_s can be obtained from as few as 10 iterations in (14).

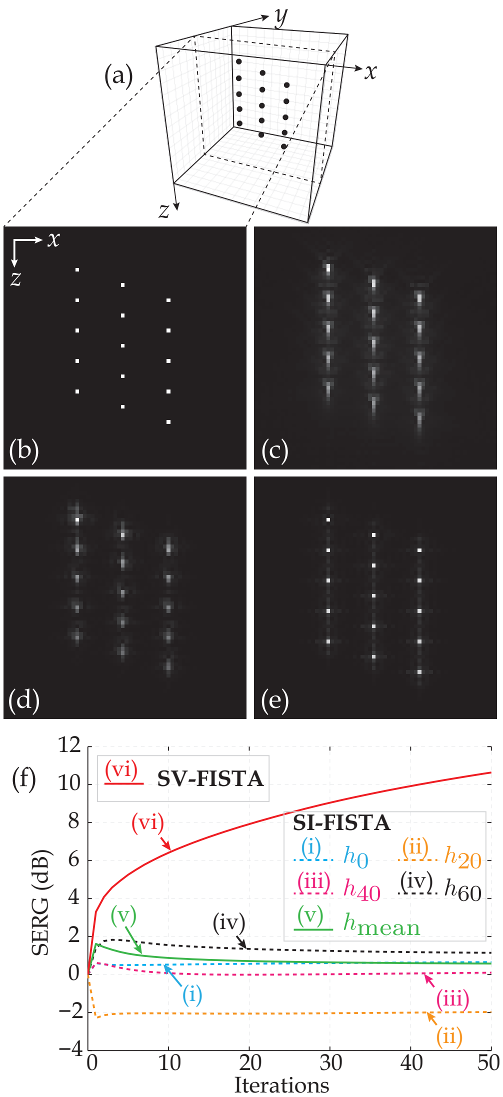

Fig. 3. Deconvolution results: (a)-(b) f_{orig}, (c) g, (d) SI-FISTA result (using h_{mean}), (e) SV-FISTA result, (f) SERG comparison.

4. EXPERIMENTAL RESULTS

In order to illustrate the performance of our algorithm, we considered a 3D stack ($64 \times 64 \times 64$) with 15 point sources located at different axial positions (Fig. 3(a-b)). We next generated $M = 64$ blurred 2D observations using the following PSF parameters (Fig. 1): objective NA = 0.9, $n_i = 1$, working distance $t_i = 1.9$mm, $n_g = 1.515$, thickness of cover-glass $t_g = 175\mu$m, $n_s = 1.33$, $\Delta x = \Delta y = 0.5\mu$m, $\Delta z = 0.8\mu$m, $\Delta d = 0.59\mu$m. We added Gaussian white noise to the blurred result (Fig. 3(c)) with noise variance set such that the blurred signal-to-noise ratio (BSNR, [7]) was equal to 40 dB.

We conducted two independent deconvolution experiments with the blurred observations. In the first case, we applied spatially-invariant FISTA deconvolution (SI-FISTA, adapted from [8] using a Level-1 cubic spline dyadic wavelet decomposition and $\lambda = 0.1$), where we used only a single 3D PSF at a time (either h_0, h_{20}, h_{40}, h_{60}, or the mean of all 64 PSFs h_{mean}, after compensating for axial-shift). Since the PSF shape varies with depth, none is appropriate; we show the volume obtained with h_{mean} after 50 iterations (Fig. 3(d)). Next, we reconstructed a volume using our proposed spatially variant FISTA deconvolution (SV-FISTA), using 64 different point spread functions, with all parameters similar to the SI-FISTA experiment. The reconstructed volumes have fewer artifacts (Fig. 3(e)). The evolution of the *signal-to-error* gain (SERG) in both experiments is shown in (Fig. 3(f)), where

$$\text{SERG}(\mathbf{f}) \triangleq 20\log_{10}\left(\frac{\|\mathbf{g}-\mathbf{f}_{\text{orig}}\|_2}{\|\mathbf{f}-\mathbf{f}_{\text{orig}}\|_2}\right). \tag{16}$$

We implemented the algorithm in Matlab (MATLAB R2011b) and ran the experiments on a Windows 64-bit machine, equipped with a dual-core Intel Xeon 3.4-GHz CPU and 16 GB RAM. The pre-computation of the sub-band dependent weight constants (α_s) for the given set of parameters was done using 10 iterations of the power method in (14), which took about 1 minute per iteration. Note that computation of these weights is only required once for a given imaging setup (i.e. all frames of a time-lapse would use the same weights). The iterative image reconstruction process took about 5.5 seconds per iteration, of which 5 seconds were spent computing the reblurred signal by applying $\mathbf{H}^\top\mathbf{H}$. By contrast the shift invariant method took about 0.55 seconds for each iteration. In both cases, updating the wavelet coefficients by soft-thresholding the Landweber update is computed in 0.5 seconds, since the SV filter-bank structure does not introduce any additional complexity (Fig. 2(c)). These results are in line with the theoretical complexity, whose order is M times more complex than that of the shift-invariant method. Because the computation in each of the M-channels could be done independently of that of the other channels, the workload could be delegated to a cluster of computers at each iteration to bring down the effective computation time.

5. DISCUSSION AND CONCLUSION

We have presented a fast ISTA algorithm for deconvolution problems with PSFs that are depth-variant. The algorithm naturally handles differing sampling steps associated with the blurred data stack (stage position step Δd) and the PSF kernel (Δz). Also, the multi-channel framework can handle a number of blurred z-slices (M) independent of the dimensions of the PSF kernel and reconstruction (in practice, we set $M \geq N_z$), which could even be non-uniformly spaced. Since the proposed SV-FISTA is applied to the entire dataset rather than blocks, it does not require post-processing with suitable transition masks to fuse individually deblurred regions. A limitation of our approach is that the algorithm does not handle *lateral* shift-variant PSFs. Further work will include comparison to block-wise deconvolution methods.

6. REFERENCES

[1] D. A. Agard, Y. Hiraoka, P. Shaw, and J. W. Sedat, "Fluorescence microscopy in three dimensions," *Methods In Cell Biology*, vol. 30, pp. 353–377, 1989.

[2] L. Landweber, "An iteration formula for Fredholm integral equations of the first kind," *American Journal of Mathematics*, vol. 73, no. 3, pp. 615–624, 1951.

[3] C. Preza and J. Conchello, "Depth-variant maximum-likelihood restoration for three-dimensional fluorescence microscopy," *J. Opt. Soc. Am. A*, vol. 21, no. 9, pp. 1593–1601, Sep 2004.

[4] E. Maalouf, B. Colicchio, and A. Dieterlen, "Fast deconvolution with non-invariant PSF for 3-D fluorescence microscopy," in *Proc. SPIE*, 2008, vol. 7000, pp. 70001K 1–8.

[5] M. Temerinac-Ott, O. Ronneberger, P. Ochs, W. Driever, T. Brox, and H. Burkhardt, "Multiview deblurring for 3-D images from light-sheet-based fluorescence microscopy," *IEEE Trans. Image Proc.*, vol. 21, no. 4, pp. 1863–1873, 2012.

[6] S. Ben Hadj and L. Blanc-Féraud, "Modeling and removing depth variant blur in 3D fluorescence microscopy," in *ICASSP*, 2012, pp. 689–692.

[7] C. Vonesch and M. Unser, "A fast thresholded Landweber algorithm for wavelet-regularized multidimensional deconvolution," *IEEE Trans. on Image Proc.*, vol. 17, no. 4, pp. 539–549, 2008.

[8] C. Vonesch and M. Unser, "A fast multilevel algorithm for wavelet-regularized image restoration," *IEEE Trans. on Image Proc.*, vol. 18, no. 3, pp. 509–523, 2009.

[9] T. D. Visser, J. L. Oud, and G. J. Brakenhoff, "Refractive index and axial distance measurements in 3-D microscopy," *Optik*, vol. 90, no. 1, pp. 17–19, 1992.

[10] I. Daubechies, M. Defrise, and C. De Mol, "An iterative thresholding algorithm for linear inverse problems with a sparsity constraint," *Comm. on Pure and Applied Math.*, vol. 57, no. 11, pp. 1413–1457, 2004.

[11] N. Chacko and M. Liebling, "Fast thresholded multichannel Landweber algorithm for wavelet-regularized multi-angle deconvolution," in *Proc. SPIE*, 2013, vol. 8858, pp. 885819–885819–10.

[12] A. Beck and M. Teboulle, "A fast iterative shrinkage-thresholding algorithm for linear inverse problems," *SIAM J. Img. Sci.*, vol. 2, no. 1, pp. 183–202, Mar. 2009.

[13] G. H. Golub and C. F. Van Loan, *Matrix computations*, Johns Hopkins University Press, Baltimore, MD, USA, 1996.